Open Access

Catalysis Research

LIDSEN Publishing Inc.

Original Research

Soil Treatment from Hazardous Particles Using Designed Nanosensors: A Physical and Chemical Analysis

Fatemeh Mollaamin *

Department of Biomedical Engineering, Faculty of Engineering and Architecture, Kastamonu University, Kastamonu, Turkey; E-Mail: fmollaamin@kastamonu.edu.tr

* **Correspondence:** Fatemeh Mollaamin; E-Mail: fmollaamin@kastamonu.edu.tr

Academic Editor: Rajesh Kumar Raju

Special Issue: Nanoparticles in the Catalysis

Catalysis Research
2025, volume 5, issue 1
doi:10.21926/cr.2501003

Received: November 11, 2024
Accepted: February 27, 2025
Published: March 06, 2025

Abstract

Being critical to achieving Sustainable Development Goals (SDGs) of the United Nations, strengthening understanding of the properties and processes of soil at national and regional scales is imperative. The target of this research is removing transition metals of Cr, Mn, Fe, Zn, W, Cd from soil due to nanomaterial-based boron nitride nanocage (B_5N_{10}-nc). The electromagnetic and thermodynamic attributes of toxic transition metals trapped in B_5N_{10}-nc were depicted by materials modeling. It has been studied the behavior of trapping of Cr, Mn, Fe, Zn, W, and Cd by B_5N_{10}-nc for sensing the soil metal cations. B_5N_{10}-nc was designed in the existence of transition metals (Cr, Mn, Fe, Zn, W, Cd). Case characterization was performed by the DFT method. The nature of covalent features for these complexes has represented the analogous energy amount and vision of the partial density of states between the *p* states of boron and nitrogen in B_5N_{10}-nc with and *d* states of Cr, Mn, Fe, Zn, W, Cd in X⟷B_5N_{10}-nc complexes. Furthermore, the nuclear magnetic resonance (NMR) analysis indicated the notable peaks surrounding Cr, Mn, Fe, Zn, W, and Cd through the trapping in the B_5N_{10}-nc during atom detection and removal from soil; however, it can be seen some fluctuations in the chemical shielding treatment of isotropic and anisotropy tensors. Based on the results in this research, the selectivity of toxic metal, metalloid and nonmetal elements adsorption by B_5N_{10}-

nc (atom sensor) have been indicated as: Cd > Zn > Fe > Cr > Mn ≈ W. In this article, it is proposed that toxic metal, metalloid and nonmetal elements–adsorbed might be applied to design and expand the optoelectronic specifications of B_5N_{10}-nc for generating photoelectric instruments toward soil purification. The progress in surface selectivity improvement, mainly including a number of approaches such as crosslinking, nanoparticle doping, surface modification, and the use of unique synthetic methods, is summarized. These approaches are promising for ion-exchange membrane synthesis for electrodialysis, alternative energy, and valuable component extraction from natural or contaminated soil.

Keywords
Nanomaterial; soil contamination; B_5N_{10}-nc; molecular modeling; DFT

1. Introduction

Numerous studies have examined the removal of heavy metals and organic-pollutants from different types of systems. Still, none of them have addressed the removal of these co-occurring heavy metals and organic pollutants and the use of microbes to do so. Therefore, the main focus of this review is on the recent developments in the concurrent microbial degradation of organo-pollutants and heavy metal removal [1].

Heavy metals remark to some metals and metalloids having biological toxicity like Cd, Hg, As, Pb, and Cr [2]. Heavy metal contamination of soil and the environment has been accelerated in modern society due to industrialization, rapidly expanded world population, and intensified agriculture. Accumulation of heavy metals often results in soil/water degradation and ecosystem malfunction. Moreover, heavy metals enter food chains from polluted soil, water, and air, and consequently cause food contamination, thus posing a threat to human and animal health [3-5]. Trace metals in soils and dust can accumulate in the human body via direct inhalation, ingestion, and dermal contact absorption [6-9] or the soil-crop system [10, 11]. The anthropogenic sources of metals include traffic emission, industrial and domestic emission, atmospheric deposition, mining, waste disposal, sewage, pesticides, and fertilizers [12-15]. Without proper management, abandoned mines will cause more serious environmental impacts than active mines [16]. Consumption of food crops growing in contaminated area is one of the important sources of human exposure to metals in mining areas [17-19].

Soil contamination in the urban environment by trace metals is of public concern. For better risk assessment, it is important to determine their background concentrations in urban soils. For instance, Molybdenum (Mo) is an essential trace element for human, animal, and plant health. Mo deficiency in soils has frequently been reported, especially under P-deficient conditions. However, Mo is also a potentially toxic contaminant to soils and aquifers that may pose a significant threat to ecological and human health [20]. Another research studied the sources and extent of arsenic (As) contamination and the translocation and speciation from microbes to soil are illustrated [21]. Moreover, several activities can build up soil copper (Cu) concentrations, leading to incorporation into the food chain and adversely affecting natural and managed ecosystems [22]. The cobalt (Co)-contaminated soil has exposed potential toxicity to humans, plants, and animals. Recently, scientists

have summarized the natural and anthropogenic sources arousing the increase of cobalt in soil and reviewed the cobalt species in soil and factors that influence the mobilization of cobalt [23].

Soil contamination in urban environment by trace metals is of public concerns. For better risk assessment, it is essential to determine their background concentrations in urban soils. One investigation determined the concentrations of 9 trace metals including As, Ba, Cd, Co, Cu, Ni, Pb, Se, and Zn in 214 urban soils from 6 cities of different sizes from both public and commercial sites in Florida [24].

Toxic heavy metals, organic pollutants, and emerging contaminants, as well as other biotic and abiotic stressors, can all affect nutrient availability, plant metabolic pathways, agricultural productivity, and soil fertility. Microbes can inhibit THMs uptake, degrade organic pollutants, and release biomolecules that regulate crop development under drought, salinity, pathogenic attack, and other stresses. Despite the fact that root exudates have the potential to attract selected microorganisms and biochar, there has been little attention paid to these areas, considering that this work addresses a critical knowledge gap of rhizospheric engineering-mediated root exudates to foster microbial and biochar adaptation [25].

Boron nitride nanomaterials have been used owing to their unique characteristics, such as eco-friendly attributes for pollutant adsorption, big surface area, high chemical & mechanical strength, and semiconducting properties [26-29]. Boron nitride nanomaterials usually exhibit semi-leading behavior, which is considered a proper alternative to carbon nanotubes. The properties of boron and nitrogen atoms, which are the first neighbors of carbon in the periodic table, make boron nitride an interesting subject of numerous studies [30-32]. In recent years, different investigations on the adsorption of chemical contaminants and applying various boron nitride nanomaterials as adsorbents for water purification have been studied [33-35].

Various physical shapes of boron nitride (BN)-based nano adsorbents such as nanoparticles, fullerenes, nanotubes, nanofibers, nanoribbons, nanosheets, nanomeshes, nanoflowers, and hollow spheres have been broadly considered possible adsorbents owing to their exceptional characteristics such as large surface area, structural variability, great chemical/mechanical strength, abundant structural defects, high reactive sites, and functional groups [36, 37].

In this work, B_5N_{10}-nc has been modeled for trapping transition metals of Cr, Mn, Fe, Zn, W, Cd. Physical and chemical properties of the interaction binding between Cr, Mn, Fe, Zn, W, Cd, and boron/nitrogen in B_5N_{10}-nc have been estimated.

2. Theory, Substances, and Approaches

2.1 Trapping Metal, Metalloid and Nonmetal Elements in B_5N_{10}-nc

The goal of this research article is to detect and trap the metal, metalloid and nonmetal atoms from soil by using B_5N_{10}-nc. The intention is to remove Cr, Mn, Fe, Zn, W, and Cd from the soil medium containing toxic ingredients. The soil medium consists of metal, metalloid and nonmetal atoms and the added B_5N_{10}-nc. B_5N_{10}-nc was modeled in the presence of Cr, Mn, Fe, Zn, W, Cd through computational methods of density functional method of CAM–B3LYP–D3.

The metal, metalloid and nonmetal atoms were successfully incorporated in the center of B_5N_{10}-nc toward formation of Cr↔B_5N_{10}-nc, Mn↔B_5N_{10}-nc, Fe↔B_5N_{10}-nc, Zn↔B_5N_{10}-nc, W↔B_5N_{10}-nc, and Cd↔B_5N_{10}-nc complexes and charge distribution of these complexes has been computed owing

to the parameter of Bader charge evaluation [38]. Irrespective of what element, the B_5N_{10}-nc becomes bigger for embedding these elements.

2.2 Method of Density Functional Theory (DFT)

There are many ions and electrons in a metallic solid, which form a many-body system. DFT has been performed in this article due to projector/ameliorated/wave method, Perdew/Burke/Ernzerhof functional based on the generalized gradient approximation as the exchange-correlation functional, and non-empirical PBE functional [39-42]. For years, discussions on metals and metalloids with computed bandwidths have been meaningful in DFT. In this paper, it has been investigated first principles calculations for trapping transition metals of Cr, Mn, Fe, Zn, W, Cd by B_5N_{10}-nc using DFT methods.

The electronic density within the Kohn-Sham (KS) equations leads us to a considerable reduction of quantum computing towards Hamiltonian parameter [43, 44]:

$$\hat{H}_s = -\sum_i^M \frac{1}{2}\overline{\nabla}_i^2 + \sum_i^M v_s(\vec{r}_i) = \sum_i^M \hat{h}_s\,; \quad \hat{h}_s = -\frac{1}{2}\overline{\nabla}_i^2 + v_s(\vec{r}_i), \tag{1}$$

where *M* is non-interactive electrons, v_s is external potential. Thus, by measuring ψ_i (single particle orbitals), the parameter of electronic densities for electrons with noninteractions will be:

$$\rho(\vec{r}) = \sum_i^M |\psi_i(\vec{r})|^2\,. \tag{2}$$

So, the total energy will be:

$$E[\rho] = \sum_i^M n_i \left\langle \psi_i \left| -\frac{1}{2}\overline{\nabla}^2 + v_{ext}(\vec{r}) + \frac{1}{2}\int \frac{\rho(\vec{r}')}{|\vec{r}-\vec{r}'|}\,\mathrm{d}\vec{r}' \right| \psi_i \right\rangle + E_{xc}[\rho] + \frac{1}{2}\sum_\beta^N \sum_{\alpha\neq\beta}^N \frac{Z_\alpha Z_\beta}{|\vec{R}_\alpha - \vec{R}_\beta|}. \tag{3}$$

Furthermore, B3LYP (Becke, Lee, Yang, Parr) is a hybrid functional of the 3-parameter basis function and LANL2DZ basis set for metals and metalloids within the DFT approach [45-50]. In addition, a new hybrid exchange–correlation functional called CAM–B3LYP was suggested which merges B3LYP and the long-range correction [51]. Moreover, the DFT functionals with the Grimme's D3 correction has been considered [52]. The approach of dispersion correction is added to Kohn-Sham density functional theory (DFT-D) with higher accuracy [53, 54]. Besides, in the DFT–D3 method of Grimme et al., the expression for the Van Der Waals (vdW)-dispersion energy-correction term is used [52]. In this work, DFT computations were accomplished by Gaussian 16 revision C.01 program package [55]. The z-matrix coordination has been built for trapping transition metals of Cr, Mn, Fe, Zn, W, Cd in soil by the B_5N_{10}-nc using GaussView 6.1 [56] via the solid model and coordination (Figure 1).

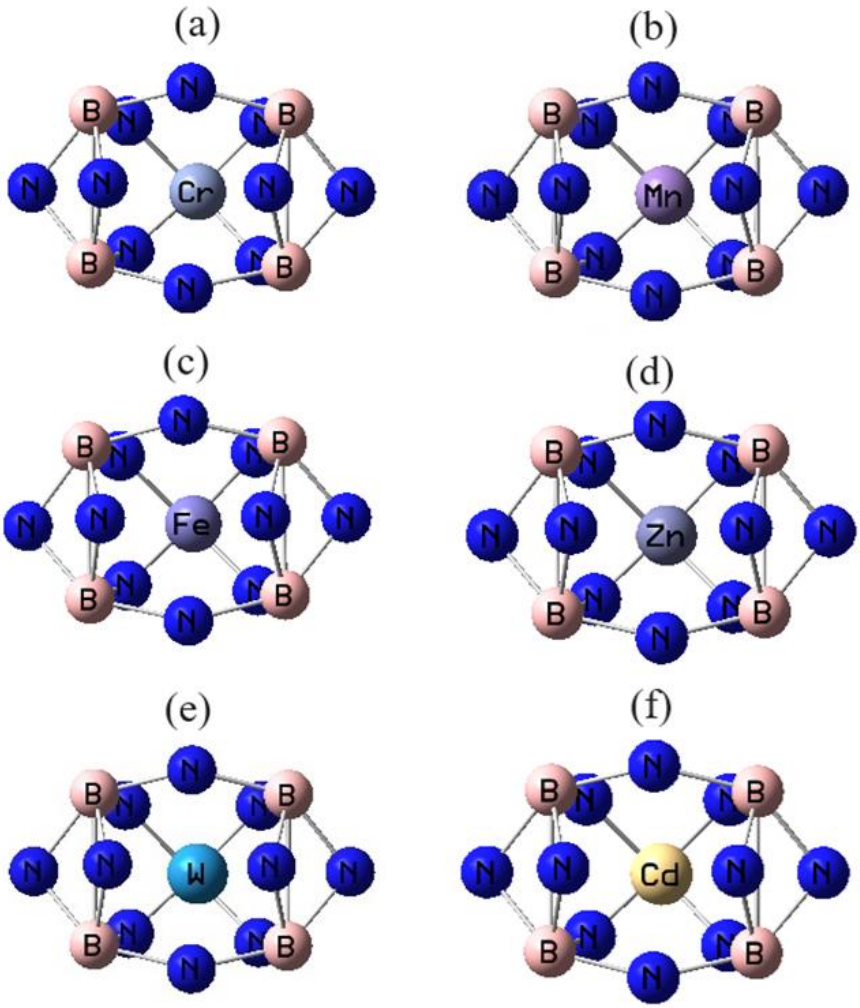

Figure 1 Optimized complexes of a) Cr↔B_5N_{10}-nc, b) Mn↔B_5N_{10}-nc, c) Fe↔B_5N_{10}-nc, d) Zn↔B_5N_{10}-nc, e) W↔B_5N_{10}-nc, and f) Cd↔B_5N_{10}-nc using CAM–B3LYP–D3/EPR–3, LANL2DZ.

The consequences will remark on the following challenges faced by the DFT approaches in accurately describing the (transition metals) - (boron and nitrogen) bonding. The adsorption status of this research was evaluated based on the simulation results. The main objective of this project was to develop a complete simulation test for eliminating soil contaminants, that can be used in future laboratory experiments.

3. Results and Discussions

B_5N_{10}-nc has been modeled for trapping transition metals of Cr, Mn, Fe, Zn, W, Cd. Physical and chemical properties of the interaction binding between Cr, Mn, Fe, Zn, W, Cd, and boron/nitrogen in B_5N_{10}-nc have been estimated.

3.1 Electronic Evaluation & PDOS

The electronic structure of toxic element trapping including Cr, Mn, Fe, Zn, W, Cd using B_5N_{10}-nc has been illustrated using CAM–B3LYP–D3/6–311+G (d,p), LANL2DZ level of theory. Figure 2(a-f) shows the projected density of state (PDOS) of X↔B_5N_{10}-nc through Cr, Mn, Fe, Zn, W, Cd

encapsulation. The existence of the energy states (*p*-orbital) of B, N, and (*d*-orbital) of Cr, Mn, Fe, Zn, W, Cd within the gap of X↔B_5N_{10}-nc induces the system's reactivity. It is clear from the figure that after trapping of transition metals, there is a significant contribution of *d*-orbital in the unoccupied level. Therefore, the curve of partial PDOS has described that *p* states of B, N atoms in B_5N_{10}-nc and *d*-orbital of Cr, Mn, Fe, Zn, W, Cd in X↔B_5N_{10}-nc overcome due to the conduction band (Figure 1 (a-f)). A distinguished adsorption trait might be seen in X↔B_5N_{10}-nc because of the potent interaction between the *p* states of boron and nitrogen in B_5N_{10}-nc with *d* states of As, Se, Co, Cu, Mo in X↔B_5N_{10}-nc complexes.

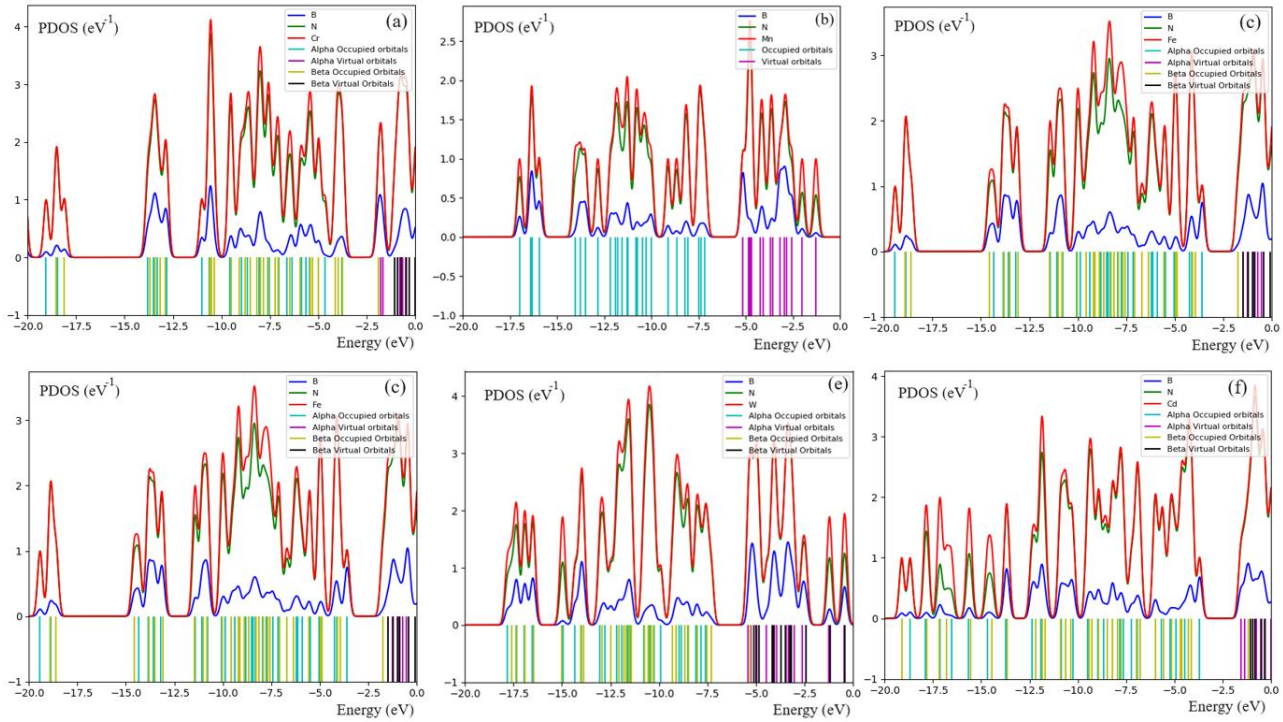

Figure 2 PDOS encapsulation of transition metals by B_5N_{10}-nc toward formation of complexes including a) Cr↔B_5N_{10}-nc, b) Mn↔B_5N_{10}-nc, c) Fe↔B_5N_{10}-nc, d) Zn↔B_5N_{10}-nc, e) W↔B_5N_{10}-nc, and f) Cd↔B_5N_{10}-nc by CAM–B3LYP–D3/6–311+G (d,p), LANL2DZ.

Figure 2(a-f) shows that Cr↔B_5N_{10}-nc, Mn↔B_5N_{10}-nc, Fe↔B_5N_{10}-nc, Zn↔B_5N_{10}-nc, W↔B_5N_{10}-nc, and Cd↔B_5N_{10}-nc complexes have the most contribution at the middle of the conduction band between -5 to -15 eV. In contrast, the contribution of boron and nitrogen states are enlarged and similar, and the grabbing of Cr, Mn, Fe, Zn, W, and Cd depicts the interfacial electronic of the B_5N_{10}-nc for selecting these atoms. Cr↔B_5N_{10}-nc has indicated one sharp peak around -10 eV for Cr in Figure 2(a), while Mn↔B_5N_{10}-nc (Figure 2b) has a sharp peak around -5 eV for Mn. The complexes of Fe↔B_5N_{10}-nc (Figure 2c) and Zn↔B_5N_{10}-nc (Figure 2d) have exhibited a sharp peak around -8.5 eV for Fe and Zn atoms, respectively. Furthermore, W↔B_5N_{10}-nc (Figure 2e) has exhibited an intense peak around -10 eV through the graphs for W. Moreover, the Cd graph in Cd↔B_5N_{10}-nc (Figure 2f) with a sharp peak around -12.5 eV attracts our attention.

As it can be seen, the order potency of atom grabbing of Cr, Mn, Fe, Zn, W, Cd by B_5N_{10}-nc based on the PDOS might be shifted as: Cd↔B_5N_{10}-nc > W↔B_5N_{10}-nc ≈ Cr↔B_5N_{10}-nc > Zn↔B_5N_{10}-nc ≈ Fe↔B_5N_{10}-nc >> Mn↔B_5N_{10}-nc. The notion of donor and acceptor bonds is a ubiquitous concept

appearing in many areas of chemistry. It is widely used for the rationalization of otherwise not easily understandable chemical properties, incredibly complex compounds. The common consensus for the TM↔B_5N_{10}-nc bonding picture remains the synergistic donation of B_5N_{10}-nc electrons via σ bonds into empty TM d orbitals and backdonation from the metal center into π* orbitals of the B_5N_{10}-nc ligands, mitigated by TM↔B_5N_{10}-nc π bonds due to the significant overlap of TM d and B_5N_{10}-nc π* orbitals. It was found that the occurrence of metal-ligand π bonds through metal d functions greatly enhances the complex stabilities.

3.2 Theoretical Insight & Analysis of Electric Potential

A nuclear quadrupole is a resonance (NQR) related to NMR that shows the unsymmetrical distribution of an electric charge of a spinning nucleus. All nuclei with a spin number ≥1 have a magnetic moment and an electric quadrupole moment that measures the deviation of the distribution of the positive charge in the nucleus [57-59]. In this work, the quantum mechanics of NQR [60-62] at zero-field containing the magnitudes of nuclear quadrupole moments have been carried out on trapping Cr, Mn, Fe, Zn, W, Cd by B_5N_{10}-nc [60-62]:

$$V(r) = V(0) + \left[\left(\frac{\partial V}{\partial x_i}\right)\Big|_0 . x_i\right] + \frac{1}{2}\left[\left(\frac{\partial^2 V}{\partial x_i x_j}\right)\Big|_0 . x_i x_j\right] + \cdots \quad (4)$$

$$U = -\frac{1}{2}\int_{\mathcal{D}} d^3 r \rho_r \left[\left(\frac{\partial^2 V}{\partial x_i^2}\right)\Big|_0 . x_i^2\right] = -\frac{1}{2}\int_{\mathcal{D}} d^3 r \rho_r \left[\left(\frac{\partial E_i}{\partial x_i}\right)\Big|_0 . x_i^2\right] = -\frac{1}{2}\left(\frac{\partial E_i}{\partial x_i}\right)\Big|_0 . \int_{\mathcal{D}} d^3 r [\rho(r) . x_i^2] \quad (5)$$

$$\chi = {}^{e^2 Q q_{zz}}/_{h} \quad (6)$$

$$\eta = {}^{q_{xx} - q_{yy}}/_{q_{zz}} \quad (7)$$

Since the electric field gradient (EFG) at the settlement of the nucleus in metal, metalloid and nonmetal atoms including Cr, Mn, Fe, Zn, W, and Cd is defined by the valence electrons bent in the pure location with familiar nuclei of B_5N_{10}-nc through trapping of Cr, Mn, Fe, Zn, W, Cd, the frequency of NQR at which intermediates occur is only for X↔B_5N_{10}-nc complexes (X = Cr, Mn, Fe, Zn, W, Cd) (Table 1 & Table 2). In the present research, the electric potential via Bader charge was estimated for Cr↔B_5N_{10}-nc, Mn↔B_5N_{10}-nc, Fe↔B_5N_{10}-nc, Zn↔B_5N_{10}-nc, W↔B_5N_{10}-nc, and Cd↔B_5N_{10}-nc complexes (Table 1 & Table 2).

Table 1 The amounts of electric potential (E_p/a.u.) and Bader charge (Q/coulomb) through NQR calculation for Cr↔B_5N_{10}-nc, Mn↔B_5N_{10}-nc, and Fe↔B_5N_{10}-nc complexes.

Cr↔B_5N_{10}-nc			Mn↔B_5N_{10}-nc			Fe↔B_5N_{10}-nc		
Atom	Q	E_p	Atom	Q	E_p	Atom	Q	E_p
B1	0.2828	-11.2393	B1	0.1887	-11.2193	B1	0.2717	-11.2441
N2	-0.2049	-18.105	N2	-0.0523	-18.282	N2	-0.1845	-18.0895
N3	-0.2541	-18.1164	N3	-0.1655	-18.3053	N3	-0.2511	-18.1138
B4	0.3299	-11.2321	B4	0.2017	-11.216	B4	0.3140	-11.2473
B5	0.3201	-11.2409	B5	0.2274	-11.2108	B5	0.3133	-11.2418
B6	0.3188	-11.2218	B6	0.1993	-11.214	B6	0.2786	-11.2448
N7	-0.1983	-18.1174	N7	-0.0548	-18.2828	N7	-0.1739	-18.1000
N8	-0.2688	-18.1262	N8	-0.1643	-18.2941	N8	-0.2434	-18.1089
N9	-0.3384	-18.1411	N9	-0.0516	-18.2949	N9	-0.3647	-18.1450
N10	-0.3121	-18.1349	N10	-0.0570	-18.291	N10	-0.3191	-18.1405
N11	-0.2881	-18.1448	N11	-0.0701	-18.2889	N11	-0.2773	-18.1317
N12	-0.3654	-18.1287	N12	-0.0798	-18.2973	N12	-0.3987	-18.1326
B13	0.1103	-11.2455	B13	0.3039	-11.2192	B13	-0.0212	-11.2706
N14	-0.1623	-18.0959	N14	-0.1153	-18.2945	N14	-0.1363	-18.0795
N15	-0.1702	-18.1124	N15	-0.1382	-18.293	N15	-0.1591	-18.0975
Cr16	1.2008	-101.752	Mn16	-0.1721	-16.5602	Fe16	1.3518	-113.9002
Zn↔B_5N_{10}-nc			W↔B_5N_{10}-nc			Cd↔B_5N_{10}-nc		
Atom	Q	E_p	Atom	Q	E_p	Atom	Q	E_p
B1	0.2799	-11.2520	B1	0.2011	-11.2204	B1	0.2777	-11.2438
N2	-0.2288	-18.1241	N2	-0.0759	-18.2918	N2	-0.2465	-18.1376
N3	-0.2132	-18.1010	N3	-0.2086	-18.3087	N3	-0.2229	-18.0972
B4	0.3237	-11.2448	B4	0.2295	-11.2118	B4	0.3237	-11.2384
B5	0.3168	-11.2466	B5	0.2541	-11.2091	B5	0.3014	-11.2511
B6	0.2980	-11.2448	B6	0.2326	-11.2120	B6	0.2946	-11.2431
N7	-0.1943	-18.1118	N7	-0.0460	-18.2929	N7	-0.2207	-18.1338
N8	-0.2260	-18.0996	N8	-0.2068	-18.3070	N8	-0.2303	-18.1073
N9	-0.3150	-18.1335	N9	-0.1994	-18.3165	N9	-0.3292	-18.1283
N10	-0.2951	-18.1390	N10	-0.1921	-18.3082	N10	-0.3202	-18.1389
N11	-0.2585	-18.1334	N11	-0.2121	-18.3019	N11	-0.2763	-18.1419
N12	-0.3695	-18.1353	N12	-0.2191	-18.3161	N12	-0.4067	-18.1296
B13	0.0617	-11.2438	B13	0.4340	-11.2307	B13	0.0513	-11.2051
N14	-0.1729	-18.1144	N14	-0.0319	-18.2847	N14	-0.1703	-18.1083
N15	-0.1664	-18.1025	N15	-0.0755	-18.2875	N15	-0.1538	-18.1018
Zn16	1.1597	-139.8870	W16	0.1162	-10.3367	Cd16	1.3286	-268.156

Table 2 The amounts of electric potential (E_p/a.u.) and Bader charge (Q/coulomb) through NQR calculation for Zn↔B_5N_{10}-nc, W↔B_5N_{10}-nc, and Cd↔B_5N_{10}-nc complexes.

Zn↔B_5N_{10}-nc			W↔B_5N_{10}-nc			Cd↔B_5N_{10}-nc		
Atom	Q	E_p	Atom	Q	E_p	Atom	Q	E_p
B1	0.2799	-11.2520	B1	0.2011	-11.2204	B1	0.2777	-11.2438
N2	-0.2288	-18.1241	N2	-0.0759	-18.2918	N2	-0.2465	-18.1376
N3	-0.2132	-18.1010	N3	-0.2086	-18.3087	N3	-0.2229	-18.0972
B4	0.3237	-11.2448	B4	0.2295	-11.2118	B4	0.3237	-11.2384
B5	0.3168	-11.2466	B5	0.2541	-11.2091	B5	0.3014	-11.2511
B6	0.2980	-11.2448	B6	0.2326	-11.2120	B6	0.2946	-11.2431
N7	-0.1943	-18.1118	N7	-0.0460	-18.2929	N7	-0.2207	-18.1338
N8	-0.2260	-18.0996	N8	-0.2068	-18.3070	N8	-0.2303	-18.1073
N9	-0.3150	-18.1335	N9	-0.1994	-18.3165	N9	-0.3292	-18.1283
N10	-0.2951	-18.1390	N10	-0.1921	-18.3082	N10	-0.3202	-18.1389
N11	-0.2585	-18.1334	N11	-0.2121	-18.3019	N11	-0.2763	-18.1419
N12	-0.3695	-18.1353	N12	-0.2191	-18.3161	N12	-0.4067	-18.1296
B13	0.0617	-11.2438	B13	0.4340	-11.2307	B13	0.0513	-11.2051
N14	-0.1729	-18.1144	N14	-0.0319	-18.2847	N14	-0.1703	-18.1083
N15	-0.1664	-18.1025	N15	-0.0755	-18.2875	N15	-0.1538	-18.1018
Zn16	1.1597	-139.8870	W16	0.1162	-10.3367	Cd16	1.3286	-268.156

Furthermore, in Table 1 & Table 2, the graph of electric potential fluctuation via Bader charge for toxic transition metals of Cr, Mn, Fe, Zn, W, and Cd grabbed by the B_5N_{10}-nc (Figure 1(a-f)) have been assessed. In Table 1 & Table 2 the trapping fluctuation of Cr, Mn, Fe, Zn, W, Cd by B_5N_{10}-nc for sensing the toxic metal, metalloid and nonmetal atoms in the contaminated soil can be observed. The graph of B_5N_{10}-nc is bent by these toxic atoms. The sharpest curves for electric potential were nominated for metal, metalloid and nonmetal atoms trapped by the B_5N_{10}-nc that prove the electron attaining of these elements aided by boron and nitrogen atoms of B_5N_{10}-nc based on the relation coefficient of R^2 as: Cd↔B_5N_{10}-nc > Zn↔B_5N_{10}-nc ≈ Cr↔B_5N_{10}-nc > Fe↔B_5N_{10}-nc > Mn↔B_5N_{10}-nc > W↔B_5N_{10}-nc (Table 1 & Table 2). The electric potential illustrates how the energy of an adsorbate molecule changes as it approaches, interacts with, and adheres to the surface of an adsorbent. The decrease in electrical potential is due to the significant contribution of electrostatic energy.

3.3 Background & Application of Nuclear Magnetic Resonance (NMR)

The investigation of NMR of high- materials and other correlated-electron systems improved for conventional superconductors and d-band transition metals, alloys, and intermetallic compounds [63].

Magnetic field gradients make it feasible to tag spatial coordinates within a model. The frequencies resonance of most atoms is well segregated from each other which causes NMR to be an element-specific method. Interactions of spins with their local environment direct to spectral alterations that evoke the local geometry and physicochemical states. Therefore, the NMR spectrum of B_5N_{10}-nc for trapping metal, metalloid and nonmetal atoms containing Cr, Mn, Fe, Zn, W, and Cd

might illustrate the possibility of B_5N_{10}-nc for sensing and grabbing these toxic elements from contaminated soil toward measuring the isotropic chemical-shielding (CSI) and anisotropic chemical-shielding (CSA) [64, 65]:

$$\sigma_{iso} = (\sigma_{11} + \sigma_{22} + \sigma_{33})/3; \quad (8)$$

$$\sigma_{aniso} = \sigma_{33} - (\sigma_{22} + \sigma_{11})/2 \quad (9)$$

The NMR quantities of isotropic (σ_{iso}) and anisotropic shielding tensor (σ_{aniso}) of Ba, As, Se, Co, Cu, Mo trapped the in the B_5N_{10}-nc towards formation of Cr↔B_5N_{10}-nc, Mn↔B_5N_{10}-nc, Fe↔B_5N_{10}-nc, Zn↔B_5N_{10}-nc, W↔B_5N_{10}-nc, and Cd↔B_5N_{10}-nc complexes was computed by Gaussian 16 revision C.01 program package [55].

Figure 3(a-f) indicated the same desire for shielding factor for boron and nitrogen; however, a remarkable deviation is observed from trapping atoms of Cr (16) (Figure 3a), Mn (16) (Figure 3b), Fe (16) (Figure 3c), Zn (16) (Figure 3d), W (16) (Figure 3e), Cd (16) (Figure 3f) through interaction with boron and nitrogen of B_5N_{10}-nc.

Figure 3 The NMR spectrum for complexes of a) Cr↔B_5N_{10}-nc, b) Mn↔B_5N_{10}-nc, c) Fe↔B_5N_{10}-nc, d) Zn↔B_5N_{10}-nc, e) W↔B_5N_{10}-nc, and f) Cd↔B_5N_{10}-nc using CAM–B3LYP–D3/LANL2DZ.

In Figure 3(a-f), toxic elements of Cr, Mn, Fe, Zn, W, Cd in the complexes of Cr↔B_5N_{10}-nc (Figure 3a), Mn↔B_5N_{10}-nc (Figure 3b), Fe↔B_5N_{10}-nc (Figure 3c), Zn↔B_5N_{10}-nc (Figure 3d), W↔B_5N_{10}-nc (Figure 3e), and Cd↔B_5N_{10}-nc (Figure 3f) describe the oscillation in the chemical shielding during atom capture. Figure 3(a-f) defines the chemical shielding between boron/nitrogen in B_5N_{10}-nc and metal, metalloid and nonmetal atoms. Thus, it may be brought up that the turnover of electron admitting for the captured toxic atoms in the B_5N_{10}-nc is Cd > Zn > Fe > Mn > Cr ≈ W that proves the strength of covalent bond across boron/nitrogen and these elements toward atom catching.

The curves of metal, metalloid, and nonmetal elements of Cr, Mn, Fe, Zn, W, and Cd through the trapping in the B_5N_{10}-nc during atom detection and removal from soil. Probing the central metal with NMR can provide information on the geometrical and electronic structure of transition-metal compounds. Accurate quantum-chemical computations of the salient metal NMR parameters can be a valuable complement to experiments, which are frequently plagued by low sensitivity, poor resolution or other fundamental problems, particularly for quadrupolar nuclei. Current computational approaches are mainly rooted in density functional theory and face different challenges, namely the proper choice of the exchange-correlation functional and the treatment of relativistic, solvation, and dynamical effects.

3.4 Interpreting Infrared (IR) Spectra

Trapping metal, metalloid, and nonmetal elements of Cr, Mn, Fe, Zn, W, and Cd in the B_5N_{10}-nc have been evaluated by IR spectroscopy during atom sensing in soil. The complexes of Cr↔B_5N_{10}-nc (Figure 4a), Mn↔B_5N_{10}-nc (Figure 4b), Fe↔B_5N_{10}-nc (Figure 4c), Zn↔B_5N_{10}-nc (Figure 4d), W↔B_5N_{10}-nc (Figure 4e), and Cd↔B_5N_{10}-nc (Figure 4f) have been analyzed through the IR spectroscopy.

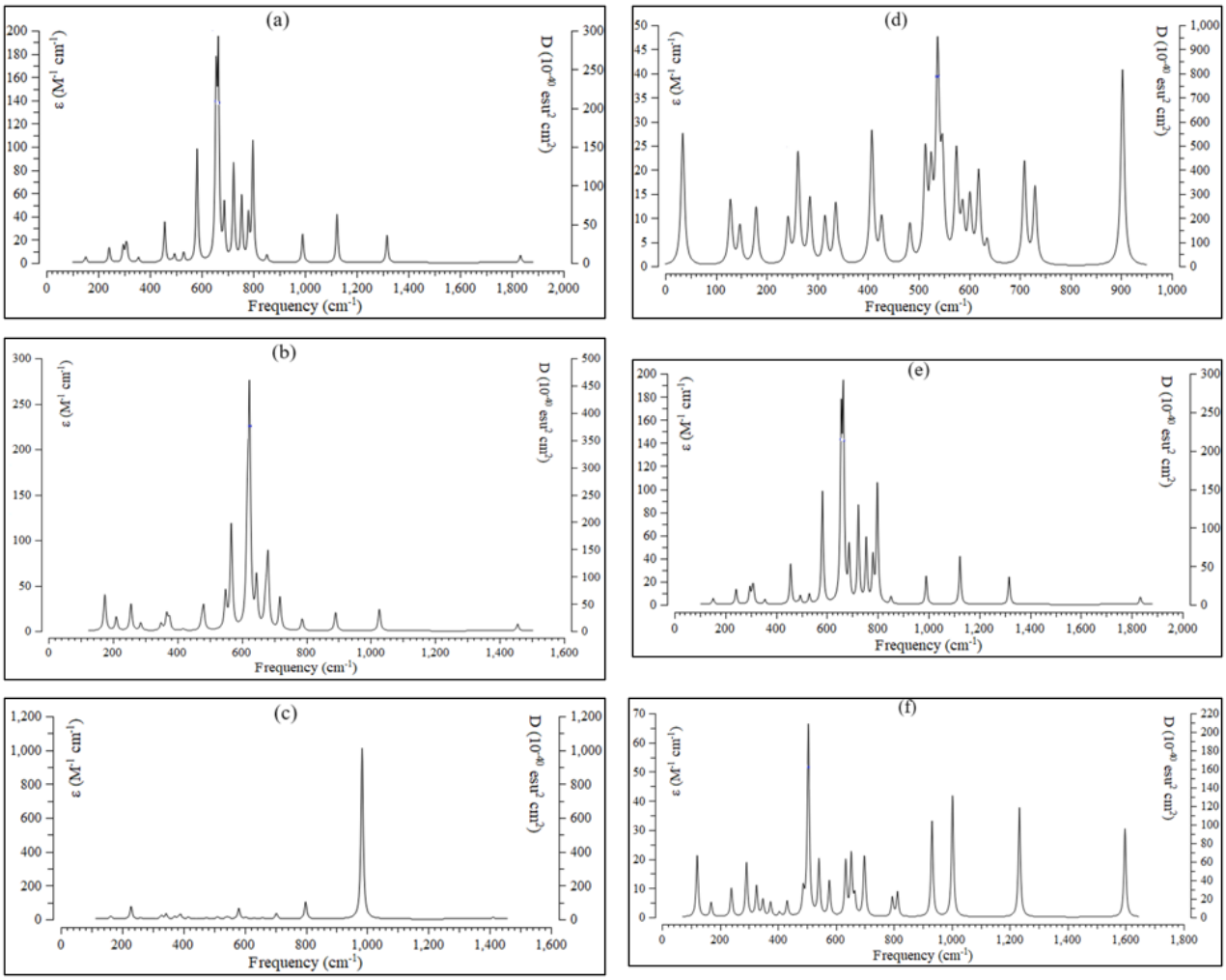

Figure 4 IR spectra for complexes of a) Cr↔B_5N_{10}-nc, b) Mn↔B_5N_{10}-nc, c) Fe↔B_5N_{10}-nc, d) Zn↔B_5N_{10}-nc, e) W↔B_5N_{10}-nc, and f) Cd↔B_5N_{10}-nc complexes.

The graph of Figure 4(a) has been shown the frequency of about 200–1800 cm^{-1} for Cr↔B_5N_{10}-nc with several sharp peaks around 655.26, 691.58, and 714.46cm^{-1}. Then, Figure 4(b) shows the frequency limitation across 200–1100 cm^{-1} for Mn↔B_5N_{10}-nc with several sharp peaks around 567.21, 616.88, 623.54, and 680.89 cm^{-1}. Figure 4(c) indicates the frequency around 1800–1100 cm^{-1} for Fe↔B_5N_{10}-nc with one sharp peak around 983.42 cm^{-1}. Figure 4(d) shows the fluctuation frequency between 50–950 cm^{-1} for Zn↔B_5N_{10}-nc with two sharp peaks around 537.66 and 902.68 cm^{-1}. Figure 4(e) indicates the frequency fluctuation between 200–1400 cm^{-1} for W↔B_5N_{10}-nc with several sharp peaks around 582.28, 656.11, 664.63, 723.76, and 798.39 cm^{-1}. Figure 4(f) shows the frequency range between 100–1600 cm^{-1} for Cd↔B_5N_{10}-nc with several sharp peaks around 504.75, 1002.32, and 1233.14cm^{-1}. Table 3 has described that B_5N_{10}-nc owing to capture transition metals including Cr, Mn, Fe, Zn, W, Cd might be more efficient detector for sensing and catching these elements from soil. For such a purpose, classical infrared spectroscopy can give valuable structural information derived from analysis of the wavenumber shifts undergone by meaningful vibrational modes of the adsorbed molecule, and from the (relative) intensity of the corresponding IR absorption bands.

Table 3 The thermochemical characters of Cr↔B_5N_{10}-nc, Mn↔B_5N_{10}-nc, Fe↔B_5N_{10}-nc, Zn↔B_5N_{10}-nc, W↔B_5N_{10}-nc, and Cd↔B_5N_{10}-nc complexes.

Compound	Dipole moment (Debye)	ΔE° × 10^{-3} (kcal/mol)	ΔH° × 10^{-3} (kcal/mol)	ΔG° × 10^{-3} (kcal/mol)	S° (cal/K.mol)
B_5N_{10}-nc	0.2020	-420.550	-420.549	-420.579	100.650
Cr↔B_5N_{10}-nc	0.6941	-1063.754	-1063.754	-1063.782	94.375
Mn↔B_5N_{10}-nc	0.4888	-485.602	-485.602	-485.629	90.852
Fe↔B_5N_{10}-nc	1.4484	-1199.586	-1199.585	-1199.614	95.351
Zn↔B_5N_{10}-nc	0.9416	-1518.749	-1518.748	-1518.780	105.321
W↔B_5N_{10}-nc	0.5946	-462.747	-462.746	-462.774	90.867
Cd↔B_5N_{10}-nc	0.7560	-3811.957	-3811.957	-3811.985	93.836

Table 3 introduces the ability of metal, metalloid and nonmetal elements of Cr, Mn, Fe, Zn, W, Cd trapped in the B_5N_{10}-nc through ΔG°_{ads} which is related to the covalent bond between these elements and B_5N_{10}-nc as a potent detector for soil purification.

The trapping process of metal, metalloid and nonmetal elements including Cr, Mn, Fe, Zn, W, Cd in the B_5N_{10}-nc is affirmed by the ΔG°_{ads} quantities:

$$\Delta G^{\circ}_{ads} = \Delta G^{\circ}_{X\leftrightarrow B_5N_{10}-nc} - \left(\Delta G^{\circ}_{X-grabbed} + \Delta G^{\circ}_{B_5N_{10}-nc}\right); \quad X = Cr, Mn, Fe, Zn, W, Cd. \qquad (10)$$

The dependence on the size of the atoms during interaction between the adsorbates of the metal, metalloid and nonmetal elements as the electron acceptors and the adsorbent of B_5N_{10}-nc as an electron donor in the complexes of Cr↔B_5N_{10}-nc, Mn↔B_5N_{10}-nc, Fe↔B_5N_{10}-nc, Zn↔B_5N_{10}-nc, W↔B_5N_{10}-nc, and Cd↔B_5N_{10}-nc. Therefore, the selectivity of the metal, metalloid and nonmetal elements by B_5N_{10}-nc (atom sensor) can result as: Cd > Zn > Fe > Cr > Mn ≈ W (Table 3). Regarding the resulting data in Table 3, thermodynamic models are thus used to elucidate selectivity based on the Gibbs free energy of each reaction. The more negative the change in the Gibbs free energy, the more favorable the reaction is. Using this understanding, we can predict the product selectivity of these multiple reversible reaction systems.

To reveal the micro/nano mechanism of the adsorption characteristics for anions, a comprehensive investigation can be conducted, which includes ion adsorption experiments, thermodynamic calculations, and molecular dynamic simulations. The results might indicate that the pH value and concentration of metal cations are the partners in determining anions' adsorption capacity. Furthermore, elevated temperature not only promotes the thermal movement of ions but also decreases the cation concentration and pH value. Besides, to prevent dissociation and volatilization, nitrogen overpressures are required during processing and/or operation at higher temperatures.

4. Conclusion

Metal nanoclusters are a type of ultrasmall nanomaterials with unique physicochemical properties. Novel nanocomposites with exciting new and sometimes exotic properties can be created by combining metal NCs with other functional materials, greatly expanding the range of possible applications. B_5N_{10}-nc can capture metal, metalloid and nonmetal elements from soil

because of electrostatic interactions between metal, metalloid and nonmetal elements and B_5N_{10}-nc. The thermochemistry and electromagnetic parameters of Cr, Mn, Fe, Zn, W, and Cd absorbed B_5N_{10}-nc has been illustrated by the DFT method. The consequences have defined that Cr, Mn, Fe, Zn, W, and Cd trapped in B_5N_{10}-nc are relatively fixed, with the most stable adsorption site in the center of the B_5N_{10}-nc system. Catching Cr, Mn, Fe, Zn, W, and Cd in the B_5N_{10}-nc happens due to the chemisorption phenomenon. The n-grabbing behavior can be found in B_5N_{10}-nc after the adsorption of Cr, Mn, Fe, Zn, W, and Cd. The work function of B_5N_{10}-nc has remarkably exhibited the transition metals adsorption with the maximum amount for the Cd > Zn > Fe > Cr > Mn ≈ W -adsorbed B_5N_{10}-nc system. However, a more detailed examination of metal solutions and biomass characteristics can be estimated for the proper understanding of the ionic competition effects. Moreover, it is proposed that transition metals-adsorbed can be employed to design and progress the optoelectronic specification of B_5N_{10}-nc for inventing photoelectric instruments. Soil science knowledge and research significantly contribute to food and nutritional security, human well-being, nature conservancy, and global peace and harmony. Achieving critical SDGs by 2030 can be facilitated by soil restoration and sustainable management.

Acknowledgments

In successfully completing this paper and its research, the author is grateful to Kastamonu University.

Author Contributions

The author did all the research work for this study.

Competing Interests

The authors have declared that no competing interests exist.

References

1. Upadhyay SK, Rani N, Kumar V, Mythili R, Jain D. A review on simultaneous heavy metal removal and organo-contaminants degradation by potential microbes: Current findings and future outlook. Microbiol Res. 2023; 273: 127419.
2. Li C, Zhou K, Qin W, Tian C, Qi M, Yan X, et al. A review on heavy metals contamination in soil: Effects, sources, and remediation techniques. Soil Sediment Contam. 2019; 28: 380-394.
3. Mollaamin F, Monajjemi M. Determination of GaN nanosensor for scavenging of toxic heavy metal ions (Mn^{2+}, Zn^{2+}, Ag^{+}, Au^{3+}, Al^{3+}, Sn^{2+}) from water: Application of green sustainable materials by molecular modeling approach. Comput. Theor. Chem. 2024; 1237: 114646.
4. Rahman SH, Khanam D, Adyel TM, Islam MS, Ahsan MA, Akbor MA. Assessment of heavy metal contamination of agricultural soil around Dhaka Export Processing Zone (DEPZ), Bangladesh: Implication of seasonal variation and indices. Appl Sci. 2012; 2: 584-601.
5. Thuy HT, Tobschall HJ, An PV. Distribution of heavy metals in urban soils–A case study of Danang-Hoian Area (Vietnam). Environ Geol. 2000; 39: 603-610.

6. De Miguel E, De Grado MJ, Llamas JF, Martin-Dorado A, Mazadiego LF. The overlooked contribution of compost application to the trace element load in the urban soil of Madrid (Spain). Sci Total Environ. 1998; 215: 113-122.
7. Madrid L, Díaz-Barrientos E, Madrid F. Distribution of heavy metal contents of urban soils in parks of Seville. Chemosphere. 2002; 49: 1301-1308.
8. Meza-Montenegro MM, Gandolfi AJ, Santana-Alcántar ME, Klimecki WT, Aguilar-Apodaca MG, Del Río-Salas R, et al. Metals in residential soils and cumulative risk assessment in Yaqui and Mayo agricultural valleys, northern Mexico. Sci Total Environ. 2012; 433: 472-481.
9. Sun G, Li Z, Bi X, Chen Y, Lu S, Yuan X. Distribution, sources and health risk assessment of mercury in kindergarten dust. Atmos Environ. 2013; 73: 169-176.
10. Mollaamin F, Monajjemi M. Trapping of toxic heavy metals from water by GN–nanocage: Application of nanomaterials for contaminant removal technique. J Mol Struct. 2024; 1300: 137214.
11. Sun G, Chen Y, Bi X, Yang W, Chen X, Zhang B, et al. Geochemical assessment of agricultural soil: A case study in Songnen-Plain (Northeastern China). Catena. 2013; 111: 56-63.
12. Sezgin N, Ozcan HK, Demir G, Nemlioglu S, Bayat C. Determination of heavy metal concentrations in street dusts in Istanbul E-5 highway. Environ Int. 2004; 29: 979-985.
13. Montagne D, Cornu S, Bourennane H, Baize D, Ratié C, King D. Effect of agricultural practices on trace-element distribution in soil. Commun Soil Sci Plant Anal. 2007; 38: 473-491.
14. Yu L, Xin G, Gang W, Zhang Q, Qiong S, Guoju X. Heavy metal contamination and source in arid agricultural soil in central Gansu Province, China. J Environ Sci. 2008; 20: 607-612.
15. Morton-Bermea O, Hernández-Álvarez E, González-Hernández G, Romero F, Lozano R, Beramendi-Orosco LE. Assessment of heavy metal pollution in urban topsoils from the metropolitan area of Mexico City. J Geochem Explor. 2009; 101: 218-224.
16. Ji K, Kim J, Lee M, Park S, Kwon HJ, Cheong HK, et al. Assessment of exposure to heavy metals and health risks among residents near abandoned metal mines in Goseong, Korea. Environ Pollut. 2013; 178: 322-328.
17. Liu H, Probst A, Liao B. Metal contamination of soils and crops affected by the Chenzhou lead/zinc mine spill (Hunan, China). Sci Total Environ. 2005; 339: 153-166.
18. Kim SH, Cho YM, Choi SH, Kim HJ, Choi JW. The effect of exposure factors on the concentration of heavy metals in residents near abandoned metal mines. J Prev Med Public Health. 2011; 44: 41-47.
19. Mollaamin F, Monajjemi M. Selectivity and sensitivity evaluation of embedded BN-nanostructure as a gas detector for air pollution scavenging: A theoretical study. Russ J Phys Chem B. 2024; 18: 1177-1198.
20. Motuzova GV, Minkina TM, Karpova EA, Barsova NU, Mandzhieva SS. Soil contamination with heavy metals as a potential and real risk to the environment. J Geochem Explor. 2014; 144: 241-246.
21. Al-Makishah NH, Taleb MA, Barakat MA. Arsenic bioaccumulation in arsenic-contaminated soil: A review. Chem Papers. 2020; 74: 2743-2757.
22. Poggere G, Gasparin A, Barbosa JZ, Melo GW, Corrêa RS, Motta AC. Soil contamination by copper: Sources, ecological risks, and mitigation strategies in Brazil. J Trace Elem Miner. 2023; 4: 100059.

23. Jiang M, Wang K, Wang Y, Zhao Q, Wang W. Technologies for the cobalt-contaminated soil remediation: A review. Sci Total Environ. 2022; 813: 151908.
24. da Silva EB, Gao P, Xu M, Guan D, Tang X, Ma LQ. Background concentrations of trace metals As, Ba, Cd, Co, Cu, Ni, Pb, Se, and Zn in 214 Florida urban soils: Different cities and land uses. Environ Pollut. 2020; 264: 114737.
25. Pathak HK, Chauhan PK, Seth CS, Dubey G, Upadhyay SK. Mechanistic and future prospects in rhizospheric engineering for agricultural contaminants removal, soil health restoration, and management of climate change stress. Sci Total Environ. 2024; 927: 172116.
26. Gonzalez-Ortiz D, Salameh C, Bechelany M, Miele P. Nanostructured boron nitride–based materials: Synthesis and applications. Mater Today Adv. 2020; 8: 100107.
27. Mishra NS, Saravanan P. A review on the synergistic features of hexagonal boron nitride (white graphene) as adsorbent-photo active nanomaterial. ChemistrySelect. 2018; 3: 8023-8034.
28. Mollaamin F, Monajjemi M. Structural, electromagnetic and thermodynamic analysis of ion pollutants adsorption in water by gallium nitride nanomaterial: A green chemistry application. Russ J Phys Chem B. 2024; 18: 533-548.
29. Muñoz AD, Escobedo-Morales A, Skakerzadeh E, Anota EC. Effect of homonuclear boron bonds in the adsorption of DNA nucleobases on boron nitride nanosheets. J Mol Liq. 2021; 322: 114951.
30. Shtansky DV, Matveev AT, Permyakova ES, Leybo DV, Konopatsky AS, Sorokin PB. Recent progress in fabrication and application of BN nanostructures and BN-based nanohybrids. Nanomaterials. 2022; 12: 2810.
31. Yang Y, Peng Y, Saleem MF, Chen Z, Sun W. Hexagonal boron nitride on III–V compounds: A review of the synthesis and applications. Materials. 2022; 15: 4396.
32. Davies A, Albar JD, Summerfield A, Thomas JC, Cheng TS, Korolkov VV, et al. Lattice-matched epitaxial graphene grown on boron nitride. Nano Lett. 2018; 18: 498-504.
33. Mollaamin F, Mohammadi S, Khalaj Z, Monajjemi M. Computational modelling of boron nitride nanosheet for detecting and trapping of water contaminant. Russ J Phys Chem B. 2024; 18: 67-82.
34. Chao Y, Zhang J, Li H, Wu P, Li X, Chang H, et al. Synthesis of boron nitride nanosheets with N-defects for efficient tetracycline antibiotics adsorptive removal. Chem Eng J. 2020; 387: 124138.
35. Mollaamin F, Monajjemi M. Boron nitride doped with transition metals for carbon monoxide detection: A promising nanosensor for air cleaning. Sensor Review. 2024; 44: 179-193.
36. Mollaamin F, Monajjemi M. Effect of implanted titanium, vanadium or chromium on boron nitride surface for increasing carbon monoxide adsorption: Designing gas sensor for green chemistry future. Russ J Phys Chem B. 2024; 18: 1199-1216.
37. Guo Y, Wang R, Wang P, Rao L, Wang C. Developing a novel layered boron nitride–carbon nitride composite with high efficiency and selectivity to remove protonated dyes from water. ACS Sustain Chem Eng. 2019; 7: 5727-5741.
38. Henkelman G, Arnaldsson A, Jónsson H. A fast and robust algorithm for Bader decomposition of charge density. Comput Mater Sci. 2006; 36: 354-360.
39. Blöchl PE. Projector augmented-wave method. Phys Rev B. 1994; 50: 17953-17979.
40. Perdew JP, Burke K, Ernzerhof M. Generalized gradient approximation made simple. Phys Rev Lett. 1996; 77: 3865.

41. Ziesche P, Kurth S, Perdew JP. Density functionals from LDA to GGA. Comput Mater Sci. 1998; 11: 122-127.
42. Zadeh MA, Lari H, Kharghanian L, Balali E, Khadivi R, Yahyaei H, et al. Density functional theory study and anti-cancer properties of shyshaq plant: In view point of nano biotechnology. J Comput Theor Nanosci. 2015; 12: 4358-4367.
43. Hohenberg P, Kohn W. Inhomogeneous electron gas. Phys Rev. 1964; 136: B864-B871.
44. Kohn W, Sham LJ. Self-consistent equations including exchange and correlation effects. Phys Rev. 1965; 140: A1133-A1138.
45. Becke AD. Density-functional thermochemistry. III. The role of exact exchange. J Chem Phys. 1993; 98: 5648-5652.
46. Lee C, Yang W, Parr RG. Development of the Colle-Salvetti correlation-energy formula into a functional of the electron density. Phys Rev B. 1988; 37: 785-789.
47. Mollaamin F, Monajjemi, M. Adsorption ability of Ga5N10 nanomaterial for removing metal ions contamination from drinking water by DFT. Int J Quantum Chem. 2024; 124: e27348
48. Stephens PJ, Devlin FJ, Chabalowski CF, Frisch MJ. Ab initio calculation of vibrational absorption and circular dichroism spectra using density functional force fields. J Phys Chem. 1994; 98: 11623-11627.
49. Cramer CJ. Essentials of computational chemistry: Theories and models. Chichester, England: John Wiley & Sons; 2004.
50. Vosko SH, Wilk L, Nusair M. Accurate spin-dependent electron liquid correlation energies for local spin density calculations: A critical analysis. Can J Phys. 1980; 58: 1200-1211.
51. Yanai T, Tew DP, Handy NC. A new hybrid exchange–correlation functional using the Coulomb-attenuating method (CAM-B3LYP). Chem Phys Lett. 2004; 393: 51-57.
52. Grimme S, Antony J, Ehrlich S, Krieg H. A consistent and accurate ab initio parametrization of density functional dispersion correction (DFT-D) for the 94 elements H-Pu. J Chem Phys. 2010; 132: 154104.
53. Grimme S, Ehrlich S, Goerigk L. Effect of the damping function in dispersion corrected density functional theory. J Comput Chem. 2011; 32: 1456-1465.
54. Mollaamin F, Monajjemi M. Application of nanoscale boron nitride for encapsulation of noxious transition metals (Cr, Mn, Fe, Zn, W, Cd) in soil: Physico-chemical characterization using DFT modeling. Adv Phys Res. 2025; 7: 5-28.
55. Frisch MJ, Trucks GW, Schlegel HB, Scuseria GE, Robb MA, Cheeseman JR, et al. Gaussian 16. Revision C.01. Wallingford, CT: Gaussian, Inc.; 2016.
56. Dennington RD, Keith TA, Millam JM. GaussView, version 6.0. 16. Shawnee Mission, KS: Semichem Inc.; 2016.
57. Ahluwalia VK. Nuclear Quadrupole Resonance (NQR) Spectroscopy. In: Instrumental Methods of Chemical Analysis. Cham: Springer Nature Switzerland; 2023. pp. 451-456.
58. Harbison GS. Nuclear Quadrupole Resonance. Lincoln, NE: University of Nebraska; 2002. doi: 10.1002/0471266965.com066.
59. Smith JA. Nuclear quadrupole resonance spectroscopy. General principles. J Chem Educ. 1971; 48: 39-41.
60. Garroway AN. Appendix K: Nuclear quadrupole resonance. Alternatives for Landmine Detection. Santa Monica, CA: Rand Corporation; 2003; Report MR-1608.

61. Poleshchuk OK, Kalinina EL, Latosińska JN, Koput J. Application of density functional theory to the analysis of electronic structure and quadrupole interaction in dimers of transition and non-transition elements. J Mol Struct Theochem. 2001; 574: 233-243.
62. Young HD, Freedman RA. Sears and Zemansky's University Physics with Modern Physics. 13th ed. Boston: Addison-Wesley; 2012.
63. Walstedt RE. Introduction to NMR studies of metals, metallic compounds, and superconductors. In: The NMR Probe of High-T_c Materials. Berlin, Heidelberg: Springer; 2008. pp. 13-65.
64. Sohail U, Ullah F, Binti Zainal Arfan NH, Abdul Hamid MH, Mahmood T, Sheikh NS, et al. Transition metal sensing with nitrogenated holey graphene: A first-principles investigation. Molecules. 2023; 28: 4060.
65. Caccamo MT, Sabatino G, Bennardo A, Magazù S. Infrared spectroscopy analysis of montmorillonite thermal effects. IOP Conf Ser Mater Sci Eng. 2020; 777: 012002.